

Installation and testing of a focusing mirror at beamline X28C for high flux x-ray radiolysis of biological macromolecules

Michael R. Sullivan, Sandeep Rekhi, Jen Bohon, Sayan Gupta, Donald Abel, John Toomey, and Mark R. Chance

Center for Proteomics and Mass Spectrometry and Center for Synchrotron Biosciences, Case Western Reserve University, Cleveland, Ohio 44106-4988, USA

(Received 20 July 2007; accepted 10 January 2008; published online 7 February 2008)

The NSLS X28C white-light beamline has been upgraded with a focusing mirror in order to provide increased x-ray density and a wide selection of beam shapes at the sample position. The cylindrical single crystal silicon mirror uses an Indalloy 51 liquid support bath as both a mechanism for heat transfer and a buoyant support to counter the effects of gravity and correct for minor parabolic slope errors. Calorimetric measurements were performed to verify that the calculated more than 200-fold increase in flux density is delivered by the mirror at the smallest beam spot. The properties of the focused beam relevant to radiolytic footprinting, namely, the physical dimensions of the beam, the effective hydroxyl radical dose delivered to the sample, and sample heating upon irradiation, have been studied at several mirror angles. © 2008 American Institute of Physics.

[DOI: [10.1063/1.2839027](https://doi.org/10.1063/1.2839027)]

I. INTRODUCTION

Beamline X28C, administered and operated by the Case Western Reserve University Center for Synchrotron Biosciences at the National Synchrotron Light Source (NSLS) (Brookhaven National Laboratory, Upton, NY), is a facility dedicated to synchrotron x-ray radiolysis studies involving investigation of the structure and function of biological macromolecules.¹ This technique, also referred to as “synchrotron footprinting” utilizes a broad-spectrum x-ray beam to rapidly generate hydroxyl radicals in a sample solution under physiological conditions (Fig. 1). These radicals then specifically modify solvent-exposed side chains of amino acids of proteins and break phosphodiester bonds in nucleic acids,^{2,3} which then serve as probes of solvent accessibility. The extents of these reactions are followed by mass spectrometry and sequencing gel electrophoresis for proteins and nucleic acids, respectively. The details of the synchrotron footprinting methodology and its use in examining the structural features and kinetics of a variety of important cellular phenomena, including RNA folding, protein-nucleic acid interactions, protein folding, protein-protein interactions, and enzymatic reactions, have been reported.¹

Investigation of increasingly complex systems invariably presents technical challenges.^{1,4-6} These large macromolecular complexes and many of the buffer constituents required for retention of a native state often serve as scavengers of the hydroxyl radical population, decreasing the occurrence of useful reactions.¹ Because the key parameter in the generation of hydroxyl radicals is the number of photons incident on the sample solution, in order to overcome the attenuating factors and produce measurable modifications in these systems, extended exposure times have been required.¹ Unfortunately, lengthy exposure to x-rays results in deleterious effects such as secondary oxidation and an increase in the dead time of time-resolved experiments. To surmount this prob-

lem, an increase in x-ray flux density is required in order to provide the same number of photons during shorter exposure times. Thus, the most important beamline development in the past year has been the installation of a cylindrical toroidal mirror for focusing the x-ray beam to increase the flux density. The main topic of this manuscript is to investigate the effect of the introduced optical component on the beam properties as relevant to radiolysis. We have described the new beamline configuration with the mirror and its mode of operation, as well as its effect on sample radiolysis in the presence of radical scavengers. Also included are results from experimental and theoretical investigations performed to understand the beam properties after the introduction of the mirror in the beam path.

II. BEAMLINE CONFIGURATION

The synchrotron footprinting technique was first developed at the X19C beamline of the NSLS in 1994 and then applied to the study of RNA folding at the X9A beamline.^{7,8} The X9A beamline was used for 4 years until the commissioning of the X28C beamline in 2000. Since then, X28C, a bending magnet beamline, has been dedicated solely to synchrotron footprinting research.

The main components of beamline X28C are shown in Fig. 2. X28C is a white-light beamline that accepts 6 mrad of the horizontal radiation emanating from the x-ray source. The beamline shares the machine ultrahigh vacuum (UHV) until the first high-purity beryllium window (0.01 in. thick), installed 8.96 m from the source. This window is mounted to a tapered Cu aperture, with 5 mm vertical by 123 mm horizontal exit dimensions. Immediately downstream is a horizontally and vertically focusing mirror located 9.378 m from the source. A 3.25 m section of the vacuum beam pipe is translated to accommodate the reflected beam. The second 0.01 in. thick Be window is attached to a five way instru-

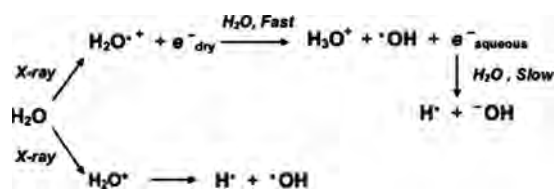


FIG. 1. Schematic representation of hydroxyl radical generation by radiolysis of water by x-ray radiation (Ref. 3).

mentation cross, which terminates the beamline UHV at X28C. This window has a boron nitride coating on the downstream surface, which is exposed to a helium atmosphere. Boron nitride is a high temperature material used to protect against oxidation of the Be windows. Since the boron nitride tends to degrade with time, the pressurized helium at the Be windows also provides a secondary measure to prevent any possible oxidation. Additionally, the helium pressure is used to monitor any leaks that can occur at the windows. A water-cooled third Be window (0.01 in. thick, also coated) is installed downstream of the exit window and a series of metal plates (0.25 in. Cu, 2 3/32 in. Pb, and 1 in. stainless steel) block stray radiation and define the beam path to a 1.5 in. diameter circular horizontal and 5 mm rectangular vertical aperture. An ~ 50 mm air gap containing the secondary shutter (preshutter) separates the exit window from the flight tube. The 0.25 in. thick stainless steel preshutter (1.7 in. wide \times 1 in. tall) blocks the beam after it exits from the third Be window at intervals during an experiment when beam is not required. This helps eliminate stray radiation and protect downstream components from overheating and excessive radiation exposure. The extendable stainless steel flight tube is sealed with a pair of coated 0.001 in. thick Be windows and also contains a pressurized helium atmosphere. A user inter-

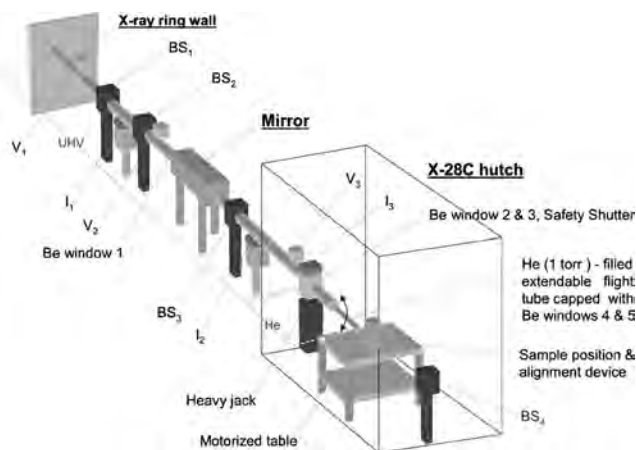


FIG. 2. Schematic representation of the configuration of beamline X28C. The position of ion pumps and gauges (I), bremsstrahlung shields (BS), valves (V), beryllium (Be) windows and location of the sample and the alignment device on the precision motorized table inside the X28C hutch are indicated. The focusing mirror resides between x-ray window 1 and BS3. The straight arrows indicate the pathway of the x-ray beam. The bidirectional curved arrow indicates the movement of the beam pipe by the heavy jack during mirror operation which allows positioning of the beam on the sample. The mirror operation, beam alignment, and sample exposure are controlled by a motor controlled unit situated outside the hutch (not shown in the figure).

lock system is connected to monitor the helium pressure and the water flow. The inner diameter of the flight tube is 1 3/8 in., defining the maximum horizontal beam size. The sample position is located 135 mm from the end of the flight tube (as depicted in Fig. 2), at a total distance of 15.568 m from the source.

X28C is equipped with a 2×3.8 m² hutch, sufficient to house all experimental equipment. The equipment and protocols at the synchrotron footprinting beamline have been continuously refined since the initiation of the program in 1996 at beamline X9A. Currently, two sets of equipment comprise the primary experimental apparatus: (1) A programmable millisecond time scale electronic shutter (Uniblitz Shutter, model No. XPS6S2P1, Vincent Associates, USA) and multiple sample holder for steady-state experiments and (2) a KinTek® quench-flow mixing device for kinetics and flow experiments that allows precise control of samples through the x-ray beam. A detailed explanation of the apparatus design and experimental techniques has been reported elsewhere.^{7,8}

III. MIRROR DESIGN SIMULATIONS

Advanced Design Consulting (ADC) USA, Inc., in collaboration with the Case Center for Synchrotron Biosciences, designed a bendable mirror for the X28C beamline. The mirror substrate design was initially based on that of the X21 beamline;⁹ the mounting system is entirely novel. The mirror design was analyzed using the program SHADOW (Nanotech-Wisconsin, University of Wisconsin), a general purpose ray tracing code specifically designed for synchrotron radiation beamline optics. The program was used to simulate the beam in order to predict the minimum spot size, beam shape, and, in conjunction with theoretical calculations,¹⁰ the possible increases in flux density for a variety of mirror settings. Figure 3 indicates that the calculated point focus spot size delivered by the mirror has a generally Gaussian shape with a full width at half maximum (FWHM) of 0.57 mm in the vertical and horizontal dimensions. The increased flux density into this spot size calculated from the demagnification (more than 500-fold), the losses due to mirror focus as calculated by SHADOW ($\sim 50\%$) and the reflectivity losses for mirror at the indicated angle (5.872 mrad) for the relevant energies ($\sim 20\%$ from 5 to 10 keV) (Fig. 4) is more than 200-fold. Control of horizontal size (and demagnification) is accomplished by increasing the angle of the mirror. With the mirror centered at 9.378 m from the source and with a focal position in the hutch at 15.568 m from the source, the optimum angle for the desired energy range was calculated to be 0.336° (5.872 mrad). Changing the angle of the mirror to 0.185° (3.232 mrad) increases the horizontal size of the beam considerably at the 15.568 m position. The angular change also produces a concave shape (Fig. 3), but an aperture with dimensions of 2 mm vertical and 10 mm horizontal can be used to block the unwanted rays and create a relatively uniform area of useful beam. In addition to defining the beam morphology, angular changes of the mirror alter the reflectivity and hence the total flux delivered by the mirror (Fig. 4). The combination of these effects produces a variety

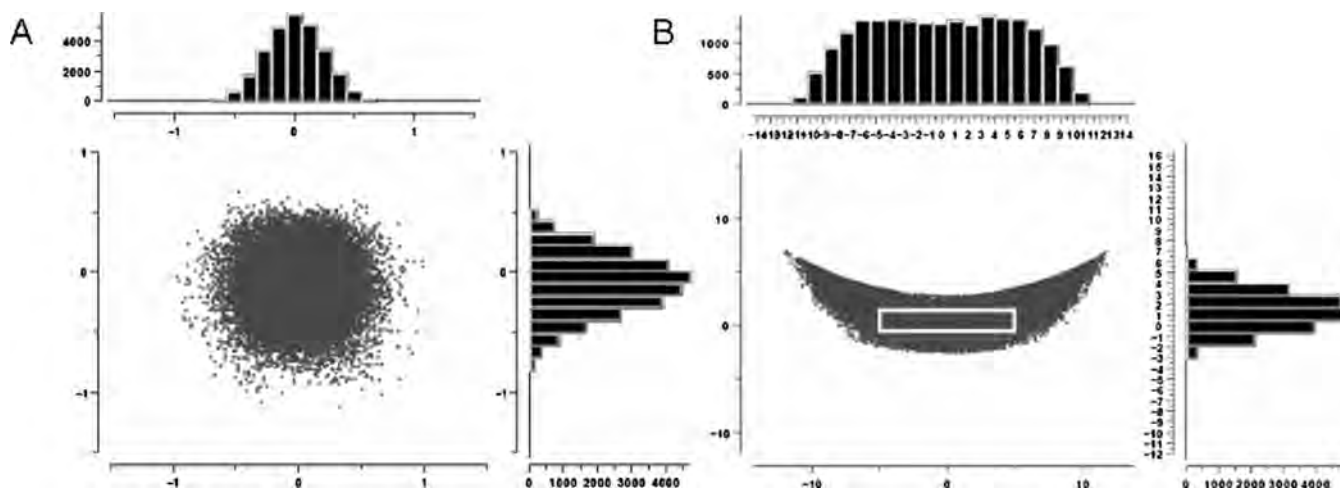


FIG. 3. SHADOW simulations at 15.568 m from the source of (A) the focused beam (5.872 mrad) and (B) a beam which accommodates the current largest sample size (3.232 mrad) (shown as superimposed $2 \times 10 \text{ mm}^2$ rectangle). Scatter plot and histogram base axes are in units of mm. Histogram dependent axes indicate the number of rays in each bin out of the 50 000 simulated.

of beam shapes and associated flux densities. These changes also result in a vertical displacement of the beam at the sample position, requiring realignment of the beamline.

IV. MIRROR CHARACTERIZATION AND INSTALLATION

Figure 5 depicts a schematic of the mirror assembly at the X28C beamline. The substrate material of the mirror is a single silicon crystal with dimensions of $50 \times 100 \times 1100 \text{ mm}^3$. The mirror has a cylindrical cut with a sagittal radius of 43.79 mm, bendable to a toroidal figure from infinite to 1.2 km meridional radius with an accuracy of $5 \mu\text{rad}$. The remaining thickness at the mirror center is 35 mm. Clamping and separate bender arms have been applied to each end of the mirror to perform the bending of the mirror into a toroid and to provide meridional focusing. The mirror collects 6 mrad (horizontal) and the full vertical solid angle from the synchrotron source, providing a horizontal beam

size of 56.3 mm at the position of the optic (9.378 m). The full beam can be collected at grazing incident angles from 3 to 8 mrad, with a calculated optimal value of 5.872 mrad, providing a point focused beam located 15.568 m downstream from the source at the steady-state sample position. dc servomotors are used for precise actuation that controls mirror movement with an x travel of $\pm 5 \text{ mm}$ and a y travel of $\pm 10 \text{ mm}$. The surface roughness of the mirror is $\leq 5 \text{ \AA}$ rms and it is coated with a 68 nm thickness Pd film via evaporation. A monolayer of chromium was used to serve for better adhesion of the coated layer on the silica substrate. Pd was chosen as the coating material due to its reflectivity cut-off energy (depending on the mirror angle), e.g., around 15 keV at 4.5 mrad, which provides abundant beam around the x-ray energies of our interest. The mirror was constructed, coated, and thoroughly inspected by Winlight System S.A. (France) and was found to be within specifications. Finite element analysis of the system, including uneven heat loading, convective cooling, gravity, and buoyancy testing, to model the effectiveness of the support and cooling

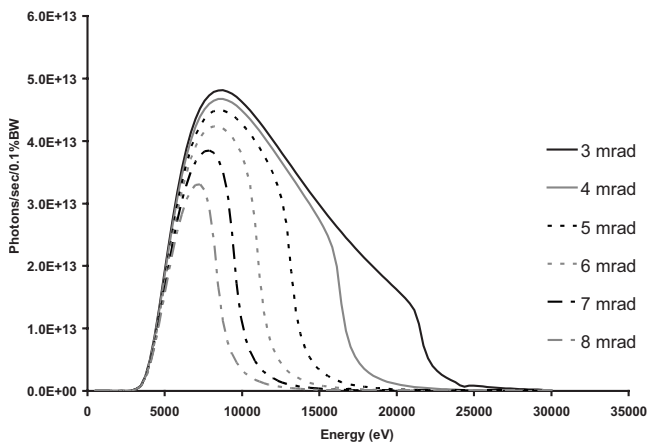


FIG. 4. X-ray flux at X28C beamline with the palladium-coated silicon mirror at different angles (Ref. 10). Calculations include NSLS bending magnet flux, transmission through 0.032 in. beryllium, a 780 mm path of 1 Torr helium, and 185 mm of air path as well as the reflectivity of the Pd coating. Flux density values can be calculated from the integrated curve divided by the spot size at a given angle.

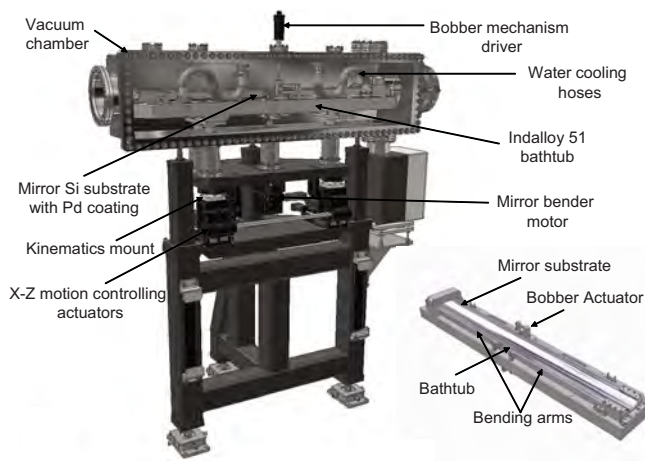


FIG. 5. (Color online) Components of the mirror assembly. The inset figure provides a top view of the mirror.

mechanism¹¹ indicates only a very small thermal and mechanical contribution to the overall slope error of the mirror. The Indalloy 51 liquid metal support has the ability to correct for minor parabolic slope errors. A bobber mechanism can be employed to displace the fluid under the mirror by ± 1.5 mm, allowing a rms slope error correction on the order of $2 \mu\text{rad}$. We have not yet found the use of this device necessary for our experiments; therefore we do not have an analysis of the bobber mechanism. The unique mounting of the mirror through flexure style bearings ensures that the contributions to slope error from errant mechanical stresses due to machining tolerances are virtually nonexistent. After correction, the surface figure error (measured minus ideal) is $\leq 0.5 \mu\text{rad}$ rms.

The mirror is secured to the 304 stainless steel “bathtub” that provides both mechanical support and water cooling to the optic (Fig. 5). The mirror operates in an UHV environment ($< 10^{-9}$ Torr); thus the entire mirror assembly is completely UHV compatible. A unique feature of this mirror system is the dual use of Indalloy 51 as both a mechanism for heat transfer and a buoyant support to negate the effects of gravity. Indalloy 51 is a commercial eutectic alloy obtained from Indium Corporation of America. This water-insoluble alloy is a lustrous, silvery liquid or gray solid metal with a mass percentage composition of Ga:In:Sn=62.5:21.5:16 and mass density of 6.5 gm/cm^3 . The melting point of this alloy is 10.7°C . Indalloy 51, with a thermal conductivity equivalent to stainless steel and virtually no contact resistance, occupies a 3 mm gap surrounding the mirror. The primary mode of heat transfer through the thin layer of liquid is conduction from the optic through the fluid into the bathtub and finally into the coolant that circulates through the integrated cooling channels. Another feature employed in shape control is the set of MACOR® pucks that line the bottom of the mirror. When the mirror is pitched to high angle, the pucks compensate for the linear taper of the buoyant force. The rigid tubular steel base provides a sound support for the vacuum chamber and the mirror manipulation mechanism. A kinematic mount is formed between the manipulating jacks and slides and the external mirror support plate through the three ball transfers (Fig. 5) and three tool-steel groove blocks. The arrangement of three jacks and two slides provides five degrees of freedom for the mirror. DC servomotors with gearheads and rotary encoders drive standard jacks and slides (ADC, Inc.). The rectangular vacuum chamber enclosing the optic opens on the front side to allow easy access to internal components. Features included on this chamber include an aluminum foil door seal, twin vacuum pump ports, a vacuum gauge port, water and vacuum guard feedthroughs, as well as two auxiliary ports. Three view ports are included in the cover at strategic places to allow observation of the critical components.

The necessary mass of Indalloy 51 was weighed out and was frozen into a funnel in an upright position. With the mirror assembly properly placed and installed, the bobber mechanism was removed and the funnel containing Indalloy was placed into the bobber hole. Using an old door seal gasket, the chamber was closed and then pumped out overnight. The Indalloy was then allowed to melt and flow under

the mirror into the bathtub containing the MACOR® pucks. The chamber was returned to atmospheric pressure and the funnel was removed by opening the chamber door. Extreme caution was taken to avoid contamination of the mirror and prevent drips from the funnel. Since aluminum does not have compatibility with Indalloy, a stainless steel syringe needle was used to inject the remaining Indalloy into the bobber hole. The total amount of material required was 1.6 kg.

The mirror was successfully installed at X28C in December of 2005. Because of space constraints, the only convenient location to install the mirror (with a required focal point at approximately 15.6 m) was at 9.378 m from the source (Fig. 2). This required construction of an electronics rack underneath the optical table in the X28B hutch to house the ion pump controllers previously located at the mirror installation site, allowing construction of the mirror chamber without changing the X28B beamline. Movable panels were also placed into the end of the X28B hutch and the front of the X28C hutch to accommodate the beam pipe movement required to accept various mirror angles. This modification of the hutches required cutting of hutch panels at the two different locations, installation of two movable steel plates at these locations, and installation of protective lead shielding. A motorized support stand (ADC, USA) in the X28C hutch was necessary to align the beam pipe and exit window with the mirror angle. As a recent upgrade, we have motorized all the necessary support stands in the beam path to enable a readjustment of hardware positions within a matter of minutes.

V. EXPERIMENTAL OBSERVATIONS

The properties of the x-ray beam have been tested with and without the presence of the mirror.¹ The results have demonstrated that the mirror is capable of delivering a high flux density x-ray beam, readily tunable in size and effective dose supplied to the sample for a given length of exposure. Calorimetric measurements were performed to verify the flux density increase provided by the mirror and the effective dose was assayed using samples containing fluorophor dye. Beam profiles were measured by scanning a photodiode masked by a $100 \mu\text{m}$ diameter tantalum pinhole across the beam using a motorized sample slide, and the general beam shape was viewed directly as a camera image of the beam (highly attenuated by sheets of aluminum) on a phosphorescent screen. Two dimensional beam profile scans for several angles are shown in Fig. 6. Only the shape of the beam incident on the target area is shown (5 mm maximum vertical due to upstream aperture), but it should be noted that due to the toroidal mirror geometry, the overall beam shape forms an arc that is concave up at low angles (below 5.872 mrad) and concave down at angles above 5.872 mrad , with a gradual beam broadening as the angle deviates further from 5.872 mrad . Due to the beam height ($> 5 \text{ mm}$), it was necessary to combine two separate scans in order to obtain the full beam profile at 5.323 mrad (normalized to beam current).

Calorimetric measurements were performed both without the mirror and with the mirror tuned to provide the small-

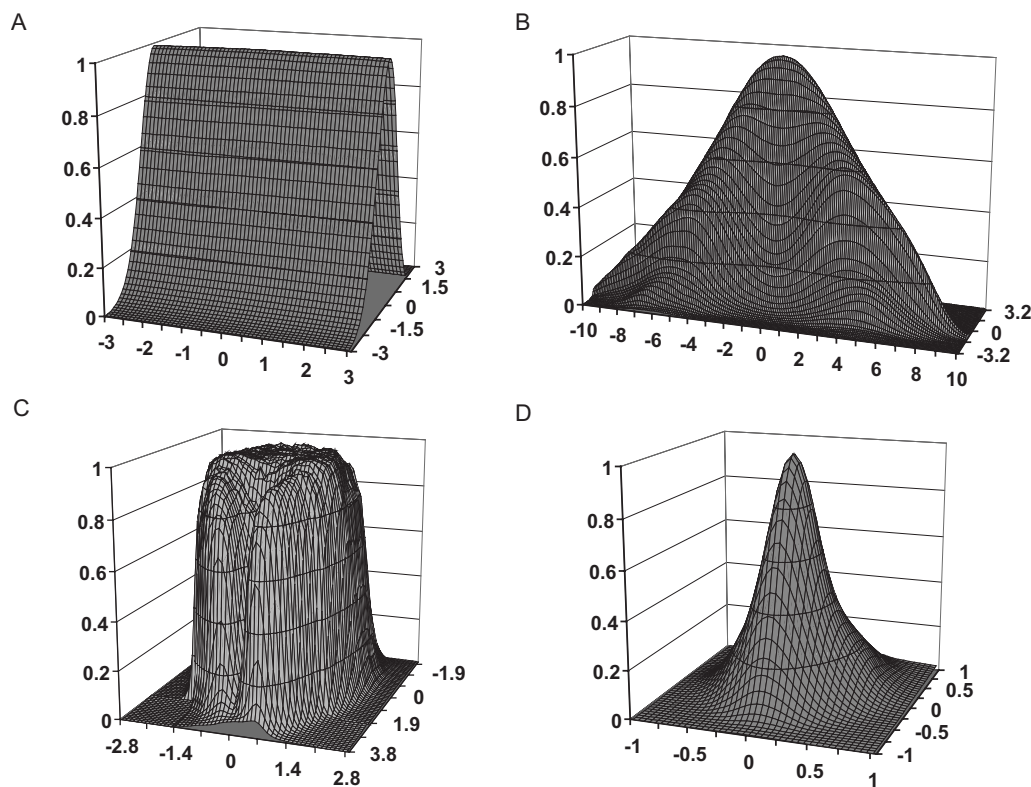


FIG. 6. Beam profiles (A) without the mirror and with the mirror at angles of (B) 3.232 mrad, (C) 5.232 mrad, and (D) 5.872 mrad (point focus). The vertical axis represents the fraction of maximum beam intensity for a given scan; both other axes are presented in mm. The profile of the beam without the mirror is measured for 6 mm of the usable horizontal width of the beam (>30 mm).

est spot size in order to measure the maximum increase in flux density delivered by the mirror. For this measurement, a copper block (349.4 g, 50.4 mm thick) with an attached K-type thermocouple was irradiated with the beam and the temperature was recorded over time with a Fluke 189 multimeter. For the measurements taken without the mirror, two different slit widths (3 and 10 mm) were used to define the unfocused horizontal beam. The vertical dimension for the unfocused beam (2.12 mm) and both vertical and horizontal (0.5 mm) dimensions for the focused beam are FWHM values for the Gaussian shape. Five experiments were performed for each setting, and values are normalized to the maximum synchrotron ring current of 300 mA and corrected for cooling effects. Thermodynamic calculations confirm that with the focused beam at its smallest spot size, the mirror is able to deliver approximately 250-fold higher power density (86.88 ± 2.740 W/mm²) than the unfocused beam (0.36 ± 0.013 W/mm²). This is in general agreement with calculations based on SHADOW simulations and the energy distribution of the beam (Fig. 4) and taking into account the smaller beam spot size, which predict an approximately 230-fold increase. In addition, because of the energy distribution, a larger percentage of the focused beam energy ($\sim 80\%$) is calculated to be deposited in a 2 mm thick aqueous sample (our current sample depth for steady-state experiments) than the unfocused beam ($\sim 50\%$). When applied to the results from the calorimetric measurements, these estimates correspond to 0.175 W/mm² deposited in the sample for the unfocused beam and 63.550 W/mm² for the focused beam—a

comparative more than 350-fold increase in useful flux density (for a 0.5 mm diameter sample surface).

The dose was assayed using samples containing the fluorophor dye Alexa 488 (Invitrogen Molecular Probes, USA). Fluorescence dyes such as Alexa are generally electron-rich aromatic compounds with a multiple ring structure which are very vulnerable to the attack by the hydroxyl radical, a highly reactive hydrophilic oxidizing agent. Oxidation may result in the breakage of the resonant ring structure, rendering the compound nonfluorescent;¹ thus the rate constants for degradation of the fluorescence signal can be used as a measure of x-ray dose on the sample. The 1.0–5.0 μ M Alexa 488 dye solutions were exposed to x-rays for 0–30 ms, and the fluorescence intensity was measured by fluorescent photometer (TBS-380 Fluorometer, Turner BioSystem). Because of the anticipated increase in dose rates, beam testing was conducted with samples containing fluorophor and either 100 mM glycerol or 20 mM adenosine 5'-triphosphate and 10 mM sodium cacodylate, buffer solutions known to scavenge hydroxyl radicals and attenuate the effective dose.¹ Dose rates are calculated as a fit to a first-order exponential decay for the degradation of fluorescence as a function of exposure time.¹ The exposure time is controlled by an electronic shutter with a minimum shutter opening time of 7 ms. At the spot focus of the beam (achieved at a 5.872 mrad angle), the mirror increases the effective dose on the sample by 123-fold, as shown by a comparison of rate constants for fluorescence decay in the presence of 100 mM glycerol before (1.6 s⁻¹) and after (197.0 s⁻¹) the installation

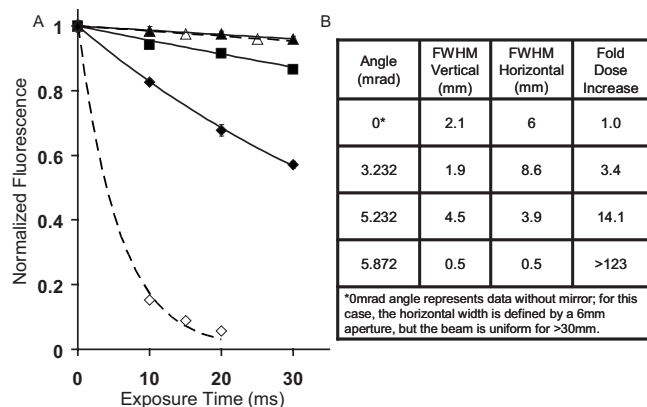


FIG. 7. Characterization of beam properties at different mirror angles. (A) Dose-response curves for reduction in Alexa 488 (in 20 mM ATP, 10 mM sodium cacodylate) fluorescence (closed symbols and solid lines) as a function of exposure time are plotted without the mirror (triangles) and with the mirror at 3.232 mrad (squares) and 5.232 mrad (diamonds) angles. Alexa 488 (in 100 mM glycerol buffer) fluorescence (open symbols and dashed lines) data are shown for the fully focused mirror at 5.872 mrad (diamonds) and prior to the installation of the mirror (triangles). (B) A table summarizing the beam size and effective dose for the tested angles.

of the mirror (Fig. 7). However, the area of the beam ($\sim 0.2 \text{ mm}^2$, with radius taken at the FWHM) at this angle is significantly smaller than our current target sample surface area ($\sim 5 \text{ mm}^2$), and therefore this increase in dose represents a minimum value. In addition to the unfocused and spot focused beams, two mirror angles allowing illumination of the entire sample surface were characterized in terms of spot size and effective dose delivered to the sample (Fig. 7). Although the vertical beam profile does not vary much at the horizontal center of the beam from the Gaussian shape of the beam without the mirror, the vertical FWHM, the horizontal beam profile, and the dose rates change dramatically with mirror angle. At 3.232 mrad, the dose rate ($4.5 \pm 0.09 \text{ s}^{-1}$) is increased 3.4-fold over the rate achieved without the mirror ($1.3 \pm 0.19 \text{ s}^{-1}$) and the horizontal FWHM is 8.6 mm, with a relatively broad peak. At 5.232 mrad, the dose rate ($18.9 \pm 0.55 \text{ s}^{-1}$) is increased by 14.1-fold, and the vertical and horizontal FWHMs of the beam are 4.5 and 3.9 mm, respectively. The angles reviewed provide parameter choices well suited to our current sample configurations, allowing tailoring of the beam to the needs of a given experiment. Prior to the installation of the mirror, the attenuating effects of large macromolecular complexes and many buffers precluded investigation via synchrotron footprinting. Similar experiments performed with the mirror at a 5.232 mrad angle yield significant hydroxyl radical modification products,¹² underscoring the necessity of the mirror in probing these complicated molecular systems.

Due to the thermally sensitive nature of many biological samples, it is important to consider the effect of the increase in flux density delivered by the mirror on the sample temperature during exposure. To investigate this, a small K-type thermocouple (surface area of $\sim 0.25 \text{ mm}^2$) was embedded in the sample. The results of this study (Fig. 8) indicate that the thermal effects are linear, with slopes that strongly depend on the mirror angle. For sensitive samples, therefore, careful

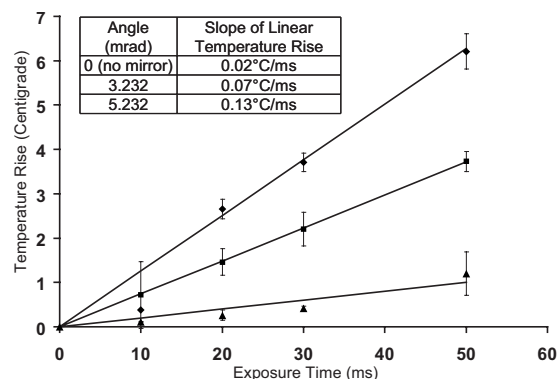


FIG. 8. The increase in sample temperature as a function of exposure time is shown without the mirror (triangles) and with the mirror at 3.232 mrad (squares) and 5.232 mrad (diamonds) angles. Linear slopes are specified in the inset table.

consideration of mirror parameters and exposure times will be required. Fortunately, the increase in dose rates due to the mirror facilitates the use of short exposure times, not only balancing thermal effects but also enabling the study of sample dynamics at the shorter time scales at which many biologically relevant processes occur. Experiments utilizing the stopped-flow apparatus can present a sample surface 0.8 mm in height and $< 0.5 \text{ mm}$ in width, allowing full use of the focused beam. This is expected to facilitate the study of rapid dynamic processes and particularly challenging samples, including research *in vivo*.

VI. SUMMARY

The state-of-the-art focusing mirror system installed at the X28C beamline delivers a high flux density and adjustably sized x-ray beam. The mirror assembly uses Indalloy 51 for heat transfer and as a buoyant support to negate the effects of gravity and has maintained stability over many hours of continuous use. The beam profile has been studied as a function of mirror angle and the minimum beam size of 0.2 mm^2 (achieved at 5.872 mrad angle) increases the power density by 245-fold and the rate constant of effective dose on the sample by more than 123-fold over the unfocused beam. The mirror has been successfully used to probe complicated molecular systems that were previously unapproachable without the mirror due to the attenuating effects of the samples.¹² Future plans at our facility include pushing the experimental range into the submillisecond regime, automated synchronization of sample to the mirror, and fully automated alignment of the beam.

ACKNOWLEDGMENTS

The authors would like to thank Dr. Steven Hulbert and Dr. James Ablett for their assistance with the selection of mirror design and specifications (BNL, NSLS). The mirror was designed by Aaron Lyndaker, Eric Johnson, and Alex Dehim (Engineer, Advance Design Consulting, USA). The fabrication and testing of the mirror substrate and coating were performed by Philippe Godefroy (CEO, Winlight Systems, S.A., France). The mirror design and installation parts of this manuscript were presented at the Ninth International

Conference on Synchrotron Radiation Instrumentation (SRI-2006).¹¹ The authors would like to thank Dr. Jeffrey Keister for his assistance with calorimetry measurements. This research is supported in part by the Biomedical Technology Centers Program of the National Institute for Biomedical Imaging and Bioengineering (P41-EB-01979).

¹S. Gupta, M. Sullivan, J. Toomey, J. Kiselar, and M. R. Chance, *J. Synchrotron Radiat.* **14**, 233 (2007).

²K. Takamoto and M. Chance, in *Encyclopedia of Molecular Cell Biology and Molecular Medicine*, edited by R. Meyers (Wiley, New York, 2004), p. 521.

³K. Takamoto and M. R. Chance, *Annu. Rev. Biophys. Biomol. Struct.* **35**, 251 (2006).

⁴T. Nguyenle, M. Laurberg, M. Brenowitz, and H. F. Noller, *J. Mol. Biol.*

359, 1235 (2006).

⁵J. G. Kiselar, R. Mahaffy, T. D. Pollard, S. C. Almo, and M. R. Chance, *Proc. Natl. Acad. Sci. U.S.A.* **104**, 1552 (2007).

⁶T. Adilakshmi, R. A. Lease, and S. A. Woodson, *Nucleic Acids Res.* **34**, E64 (2006).

⁷C. Y. Ralston, B. Sclavi, M. Sullivan, M. L. Deras, S. A. Woodson, M. R. Chance, and M. Brenowitz, *Methods Enzymol.* **317**, 353 (2000).

⁸B. Sclavi, M. Sullivan, M. R. Chance, M. Brenowitz, and S. A. Woodson, *Science* **279**, 1940 (1998).

⁹L. Yang, *Macromolecular Research* **13**, 538 (2005).

¹⁰B. L. Henke, E. M. Gullikson, and J. C. Davis, *At. Data Nucl. Data Tables* **54**, 181 (1993).

¹¹E. Johnson, A. Lyndaker, A. Deyhim, M. Sullivan, M. R. Chance, D. Abel, J. Toomey, and S. Hulbert, in *Synchrotron Radiation Instrumentation: 9th International Conference (Korea)*, edited by J. Y. Choi and S. Rah (AIP, New York, 2007), Vol. 879, p. 675.

¹²X. Xheng, P. L. Wintrode, and M. R. Chance, *Structure* **16**, 38 (2008).